Imbalanced spin-wave excitation on the exceptional line induced by anti-$\mathcal{PT}$ symmetry breaking in a ferromagnetic trilayer system

Yueting Pan,[1] Vahram L. Grigoryan,[2] Jie Yang,[3] and Ke Xia[4,*]
[1]*Beijing Computational Science Research Center, Beijing 100193, China*
[2]*Institute of Physics, Yerevan State University, Yerevan 0025, Armenia*
[3]*WaveCoRE research group, KU Leuven, Kasteelpark Arenberg 10, Leuven B-3001, Belgium*
[4]*Key Laboratory of Quantum Materials and Devices of Ministry of Education, School of Physics, Southeast University, Nanjing 211189, China*

(Received 27 May 2023; revised 5 August 2023; accepted 8 August 2023; published 24 August 2023)

We investigate the pseudo-Hermitian properties of a ferromagnet|normal-metal|ferromagnet heterojunction, where the two ferromagnets are subjected to two independently tuned magnetic fields and dissipatively coupled with one another through the ultrathin normal-metal film. The three-dimensional parameter space constituted by functions of the Gilbert damping, the enhanced damping, and the effective magnetic fields enables us to obtain the two-dimensional pseudo-Hermitian regions with different phases and an exceptional line. We find that the coalescence of two spectra occurs in one of the pseudo-Hermitian phases. Furthermore, the spin-wave excitation is highly enhanced on the exceptional line via a small circularly polarized microwave driving and the spin transfer torque induced negative Gilbert damping. Particularly, the intensity of spin-wave excitations in two subsystems could be imbalanced and adjustable to show a certain ratio through anti-parity-time (anti-$\mathcal{PT}$) symmetry breaking. Through anti-$\mathcal{PT}$ symmetry breaking, additional degrees of freedom will be generated. The method for imbalanced excitation of particles at exceptional points is also applicable to other dissipatively coupled physical systems.

DOI: 10.1103/PhysRevB.108.064428

I. INTRODUCTION

In recent years, non-Hermitian physics [1–4] has attracted considerable attention for its unprecedented phenomena and applications in optical systems [5–14], superconducting qubits [15–23], magnon-cavity systems [24–34], molecules [35–38], and other hybrid systems. Non-Hermitian systems usually have complex spectra and bi-orthogonal bases, however, some of them have real spectra when certain parameters are satisfied. As early as 1966, it was discovered that non-Hermitian systems have a unique real energy spectrum on the exceptional points (EPs) [39,40]. In the last two decades, $\mathcal{PT}$ symmetry theories have been proposed to explain the real spectra in coherent coupled (the off-diagonal coupling terms are real and positive) non-Hermitian systems [41–43]. Subsequently, more general concepts known as pseudo-Hermiticity ($\eta H \eta^{-1} = H^{\dagger}$ in which η is a Hermitian invertible operator) associated with real eigenvalues and diverse symmetries [described as $[U, H] = 0$ ($\{U, H\} = 0$) where U is a (anti-)unitary operator] have been revealed [44–46] in both coherent coupled and dissipative coupled [12,24,28–31,47] (the off-diagonal coupling terms has imaginary parts) non-Hermitian systems. The EP is included in the concept of pseudo-Hermiticity as a special situation when the two real spectra are coalescent. Recent studies have indicated that, in some particular systems, EPs can even form an exceptional line (EL) or an exceptional surface (ES) [33,48] creating an adequate range of parameter adjustment.

The dynamic exchange coupling of spin waves in the ferromagnet|normal-metal|ferromagnet ($F|N|F$) heterojunction driven by external fields [49–52] is an important system in spintronics. Since the wavelength of spin waves is as low as nanometers [53,54], the properties of the $F|N|F$ spin-pumping system, such as the synchronicity and the enhancement of spin-wave excitation at the EPs have the potential to make it a good candidate for nanoscale quantum devices [55–57]. As the first dissipative coupled system realized in spintronics [Heinrich, Tserkovnyak, Woltersdorf, Brataas, Urban, and Bauer (2003); Tserkovnyak, Brataas, Bauer. (2002)], the system is usually described by the widely studied coupled Landau-Lifshitz-Gilbert (LLG) equations [50,58,59]. So far, there has been no investigation into the theoretical characterization of its pseudo-Hermiticity. Thus, we propose a scheme for analyzing the non-Hermitian properties, especially the pseudo-Hermiticity of the system. The non-Hermitian Hamiltonian of the $F|N|F$ spin-pumping system is constructed with a complete symmetry analysis and phase identifications of states in the three-dimensional (3D) parameter space. The 3D parameter space composed of Gilbert damping, enhanced damping [58], and effective fields enables us to obtain the two-dimensional (2D) pseudo-Hermitian planes containing an EL. In our analysis, the spin pumping manifests as a dissipative coupling through dynamic exchange interaction, resulting in the coalescence [34,60–67] of energy levels in one of the pseudo-Hermitian phase.

*kexia@seu.edu.cn

 ©2023 American Physical Society

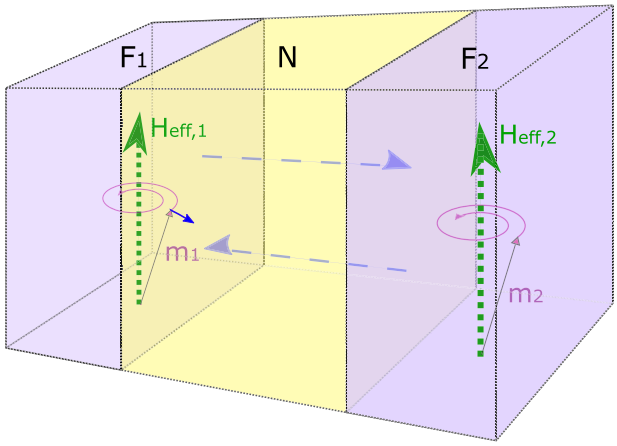

FIG. 1. The schematic picture of the system. The precession of spins in ferromagnetic films F_1 and F_2 occurs under the effective magnetic fields (green arrows). The precessing magnetic moment (lilac arrows in F_i) of spins from one ferromagnet pumps a negative damping torque $\propto \alpha_i' \mathbf{m_i} \times \dot{\mathbf{m}}_\mathbf{i}$ (short blue arrow in F_1) into the normal metal N which finally redistributed in both ferromagnets.

We find that the endpoints of the level coalescence (the region with collective dynamics) are EPs which form an EL in the pseudo-Hermitian phase plane with enhanced spin-wave excitations when negative Gilbert damping is induced. Particularly, the spin-wave excitation of two ferromagnets can be regulated unequally by enhanced damping-induced anti-$\mathcal{PT}$ symmetry breaking, while in previous times, people usually paid attention to the dynamic properties of states with unrecognized anti-$\mathcal{PT}$ symmetry. The pseudo-Hermitian analysis allows us to see the full picture of dynamics of the $F|N|F$ spin-pumping system. Our analysis may also gain insight into relevant experiments [24,50,56,68,69] through the non-Hermitian analysis.

II. MODELING

We study the $F|N|F$ structure in which two ferromagnetic films are driven by two magnetic fields, respectively, and coupled through a middle normal-metal layer. The schematic picture of the system is depicted in Fig. 1. Here, we focus on purely dissipative coupling in a collinear magnetic equilibrium configuration with small-angle excitations. On the typical timescales for electron transfer over the spacer, the magnetization dynamics are slow [50,59] due to the relatively thin N layer. The thickness for F_i represented by d_i should be thicker than transverse-spin coherence length λ_{sc} but thinner than A/J in which A is the magnetic bulk exchange stiffness and J is the Heisenberg coupling constant. Thus, F_i can completely absorb transverse spin currents [50,59]. The thickness for N should be thinner than the electron mean-free path to guarantee the ballistic electron motion, but thick enough to suppress the Ruderman-Kittel-Kasuya-Yosida (RKKY), pin-hole, and Néel-type magnetostatic interactions [50,54].

We start from the dynamic equations of the magnetization directions $\mathbf{m}_i$ described by coupled LLG equations [50]:

$$\frac{d\mathbf{m}_i}{dt} = -\gamma_i \mathbf{m}_i \times \left(\mathbf{H}_{\text{eff},i} + \frac{J\mathbf{m}_j}{M_{s,i}d_i}\right) + \alpha_i \mathbf{m}_i \times \frac{d\mathbf{m}_i}{dt} + \alpha_i' \left(\mathbf{m}_i \times \frac{d\mathbf{m}_i}{dt} - \mathbf{m}_j \times \frac{d\mathbf{m}_j}{dt}\right), \quad i, \quad j = 1, 2, \quad i \neq j, \tag{1}$$

with spin-orbit interaction induced Gilbert damping for a single ferromagnet given by α_i [59] and enhanced damping [58,59,70] given by α_i' characterizing the intensity of dynamic exchange interactions between two ferromagnets. $\alpha_i' = \gamma_i \hbar g^{\uparrow\downarrow}/(8\pi\mu_i)$ [59], where $g^{\uparrow\downarrow}$ is the dimensionless mixing conductance of the F/N interfaces, μ_i is the total magnetic moment of F_i which scales linearly with the volume of F_i. We take $\mathbf{H}_{\text{eff},i}$ as magnetic-anisotropy-dependent effective driving fields acting on F_i. The static coupling term $J\mathbf{m}_j/M_{s,i}d_i$ together with $\mathbf{H}_{\text{eff},i}$ determines effective fields experienced by the ferromagnets. The saturated magnetization for F_i is $M_{s,i}$, and the gyromagnetic ratios are γ_i.

Setting $\mathbf{m}_i \simeq \hat{\mathbf{z}} + m_{i\perp} e^{-iwt}$, where $m_{i\perp} e^{-iwt}$ denotes small deviations with precession frequency ω of the magnetization direction from its equilibrium value $\hat{z}$, the linearized dynamic equations read

$$\Omega \begin{pmatrix} m_{1\perp} \\ m_{2\perp} \end{pmatrix} = 0, \quad \Omega = \begin{pmatrix} \omega_1 + \nu_1 + i\alpha_1\omega + i\alpha_1'\omega - \omega & -\nu_1 - i\alpha_1'\omega \\ -\nu_2 - i\alpha_2'\omega & \omega_2 + \nu_2 + i\alpha_2\omega + i\alpha_2'\omega - \omega \end{pmatrix}, \tag{2}$$

in which $-\omega_i \hat{\mathbf{z}} = \gamma_i \mathbf{H}_{\text{eff},i}$, $\nu_i = \gamma_i J/M_{s,i}d_i$.

We consider a general case when α_i are positive or negative [the negative damping can be achieved by electrically [71–73] or thermally [74,75] induced spin transfer torque (STT)], while α_i' are positive, $|\alpha_i|, |\alpha_i'| \ll 1$, $\omega_1\omega_2 > 0$, $|\omega_1 - \omega_2|/|\omega_1| < 10^{-1}$. Based on the above assumptions, we construct the Hamiltonian of the system as

$$H = \begin{pmatrix} \omega_1 + i(\alpha_1 + \alpha_1')\omega_1 & -i\alpha_1'\omega_2 \\ -i\alpha_2'\omega_1 & \omega_2 + i(\alpha_2 + \alpha_2')\omega_2 \end{pmatrix},$$
$$H - \mathbb{I} \otimes \omega \simeq \Omega|_{\nu_i \to 0}, \tag{3}$$

where we take into account $\nu_i = 0$ due to the short-range nature of static coupling compared with dynamic exchange interaction when the thickness of N spacers is thick enough to weaken the static coupling but still thinner than the electron mean-free path [50,59] (the electron mean-free path of Ag, Cu, Au, Al is 53.3, 39.9, 37.7, 18.9 nm, respectively [76]), see the Supplemental Material [77] for the situation when the thickness of N spacers is thin enough so that the static coupling is sizable. The spectral matching of Eqs. (1) and (3) is also provided in the Supplemental Material [77]. By setting $\Delta = (\omega_1 - \omega_2)/2$, $\chi = [(\alpha_1 + \alpha_1')\omega_1 - (\alpha_2 + \alpha_2')\omega_2]/2$, $\varepsilon = -\alpha_1'\alpha_2'\omega_1\omega_2$ (in our system, $\varepsilon < 0$ because of $\omega_1\omega_2 > 0$,

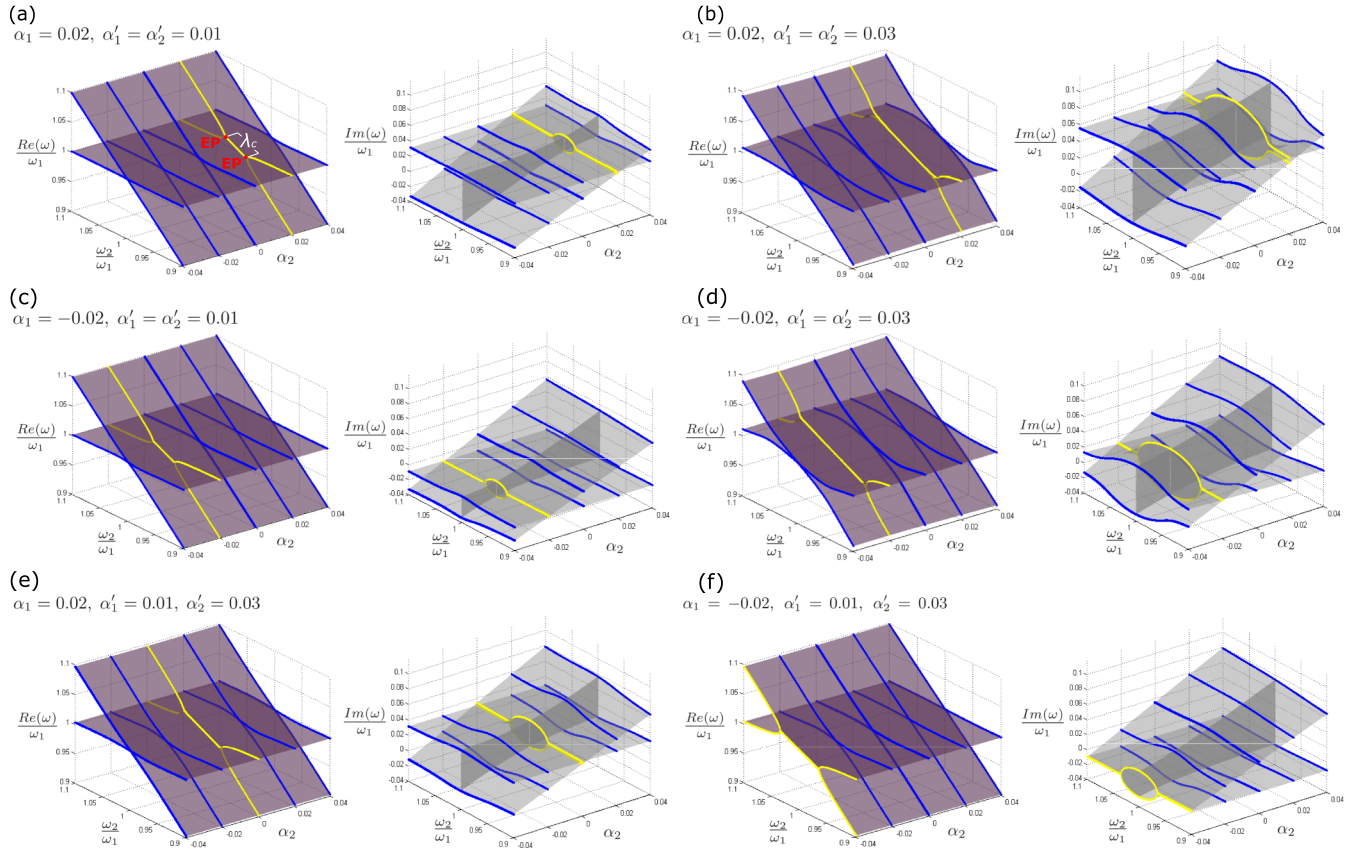

FIG. 2. Simulation of the real and imaginary part of energy levels as a function of α_2, ω_2/ω_1 with different α_1 and α_i' according to Eq. (5). Level coalescence occurs when $(\alpha_1 + \alpha_1')\omega_1 - (\alpha_2 + \alpha_2')\omega_2 = 0$ (i.e., $\chi = 0$). The coalescent length conforms to $\lambda_c \simeq 4\sqrt{\alpha_1'\alpha_2'}$.

$\alpha_i' > 0$), Eq. (3) reduces to

$$H = H_0 + \mathbb{I} \otimes [(\omega_1 + \omega_2)/2 + i\mathcal{A}],$$
$$H_0 = \begin{pmatrix} \Delta + i\chi & -i\alpha_1'\omega_2 \\ -i\alpha_2'\omega_1 & -\Delta - i\chi \end{pmatrix}, \tag{4}$$

with $\mathcal{A} = [(\alpha_1 + \alpha_1')\omega_1 + (\alpha_2 + \alpha_2')\omega_2]/2$ being the global damping of the overall system, $\mathbb{I}$ is the 2×2 identity matrix. The eigenvalues of H read

$$\omega = \pm\sqrt{\Delta^2 - \chi^2 + \varepsilon + 2i\Delta\chi} + (\omega_1 + \omega_2)/2 + i\mathcal{A}. \tag{5}$$

III. LEVEL ATTRACTION, COALESCENT LENGTH, PSEUDO-HERMITICITY, AND SYMMETRIES

We first recall the dynamic collective behavior in the system by focusing on the effects of α_i and α_i' on spectrum attraction. From Eq. (4), the coupling terms $-i\alpha_1'\omega_2$ and $-i\alpha_2'\omega_1$ are imaginary, leading to a purely dissipative coupling between F_i. We depict the real (imaginary) component $\mathrm{Re}(\omega)/\omega_1$ ($\mathrm{Im}(\omega)/\omega_1$) of the spectrum as a function of α_2, ω_2/ω_1 with distinct α_1, α_i' in Fig. 2. From Eq. (5), the level coalescence (for the real part of spectrum) occurs when

$$\Delta\chi = 0, \tag{6}$$

$$\Delta^2 - \chi^2 + \varepsilon \leqslant 0, \tag{7}$$

which results in $\mathrm{Re}(\omega) = (\omega_1 + \omega_2)/2$, $\mathrm{Im}(\omega) = \pm(-\Delta^2 + \chi^2 - \varepsilon)^{1/2} + [(\alpha_1 + \alpha_1')\omega_1 + (\alpha_2 + \alpha_2')\omega_2]/2$. The coalescence of energy levels discussed in this section refers to the same real part and different imaginary part, except for exceptional points which has the same real part and imaginary part, as indicated in Fig. 2(a). By comparing the subplots, when $\chi = 0$, namely, $(\alpha_1 + \alpha_1')\omega_1 - (\alpha_2 + \alpha_2')\omega_2 = 0$, the level attraction is most obvious; while $\Delta = 0$ ($\omega_1 = \omega_2$) has no level coalescence on the degree of ω_2/ω_1. The coalescent length (the length of the section where the real parts of energy levels are equal, i.e., the distance between the two EPs in the subplots) of spectrum follows the rule (see Supplemental Material [77] for detailed derivations)

$$\lambda_c \simeq 4\sqrt{\alpha_1'\alpha_2'}, \tag{8}$$

as indicated in Fig. 2 by the coalescent part of the yellow lines. The synchronization efficiency of the system can be controlled by adjusting α_i'.

Ignoring the scalar matrix part, the essence of H depends on the pseudo-Hermiticity and symmetry of H_0. The eigenvalue of H_0 reads

$$\omega_0 = \pm\sqrt{\Delta^2 - \chi^2 + \varepsilon + 2i\Delta\chi}. \tag{9}$$

As a 2D non-Hermitian Hamiltonian with discrete spectra and a complete bi-orthogonal system of eigenbases, H_0 is pseudo-Hermitian if and only if its spectrum is either real or

TABLE I. (Anti-)Pseudo-Hermiticities, symmetries, and EL of H_0 in the pseudo-Hermitian regions. η_+, η_- represent pseudo-Hermitian and anti-pseudo-Hermitian metrics, respectively.

Condition	(Anti-)pseudo-Hermiticity	Symmetry	Exceptional line	Phase 1	Phase 2	(Anti-)$\mathcal{PT}$ symmetry condition
$\chi = 0$ ($\varepsilon < 0$)	Anti-pseudo-Hermiticity $\eta_- H_0 \eta_-^{-1} = -H_0^\dagger$, $\eta_- = \sigma_x$	Anti-TRS† symmetry $T_- H_0^T T_-^{-1} = -H_0$, $T_- = \sigma_x T$	$\Delta^2 + \varepsilon = 0$	$\Delta^2 + \varepsilon > 0$	$\Delta^2 + \varepsilon < 0$	Anti-$\mathcal{PT}$ symmetry $\{PT, H_0\} = 0$, $P = \sigma_x$, for $\alpha_1'\omega_2 = \alpha_2'\omega_1$
$\Delta = 0$ ($\varepsilon < 0$)	Pseudo-Hermiticity $\eta_+ H_0 \eta_+^{-1} = H_0^\dagger$, $\eta_+ = \sigma_y$	TRS† symmetry $T_+ H_0^T T_+^{-1} = H_0$, $T_+ = \sigma_y T$	None	None	All	None

complex-conjugate pairs [46,78–80]. Thus, from Eq. (9), the conditions for H_0 to be pseudo-Hermitian is

$$2\chi\Delta = 0. \tag{10}$$

For $\chi = 0$ or $\Delta = 0$, the real part in the square root of Eq. (9) determines whether ω_0 is real (to be called "phase 1" throughout this work) or complex-conjugate pairs (to be called "phase 2"):

$$\begin{aligned} \Delta^2 - \chi^2 + \varepsilon > 0 &\Rightarrow \text{phase 1}, \\ \Delta^2 - \chi^2 + \varepsilon < 0 &\Rightarrow \text{phase 2}. \end{aligned} \tag{11}$$

The implications of $\Delta = 0$ and $\chi = 0$ in Eq. (1) are as follows: for $\Delta = 0$, it means $-\gamma_1 \mathbf{m}_1 \times \mathbf{H}_{\text{eff},1} = -\gamma_2 \mathbf{m}_2 \times \mathbf{H}_{\text{eff},2}$, indicating the equatability of pressing torques; for $\chi = 0$, it means $(\alpha_1 + \alpha_1')\mathbf{m}_1 \times d\mathbf{m}_1/dt = (\alpha_2 + \alpha_2')\mathbf{m}_2 \times d\mathbf{m}_2/dt$, implying the balance of damping torques in both subsystems (notice that $|\mathbf{m}_i \times d\mathbf{m}_i/dt| \propto |d\mathbf{m}_i/dt| \propto \omega_i$ for small $\alpha_{i,j}$ and $\alpha_{i,j}'$).

For $\Delta = 0$, the Hamiltonian holds TRS† symmetry (see Table I), and the spectrum is always complex-conjugate pairs because $\varepsilon < 0$, therefore, there is no phase transition in the $\Delta = 0$ plane. For $\chi = 0$, the Hamiltonian holds anti-TRS† symmetry, and the phase transition is shown in Fig. 3(a), where the pseudo-Hermitian phase 1 (phase 2) are shown by yellow (blue), and the red line between them denotes the EL. We show the real and imaginary components of the spectrum for $\chi = 0$ in Figs. 3(b) and 3(c).

H_0 is η-pseudo-Hermitian when it satisfies Eq. (10), where the metric η does not have to be unique [81]. In phase 1, H_0 satisfies $\eta H_0 \eta^{-1} = H_0^\dagger$, and one of the expressions of η is

$$\begin{aligned} \eta &= (DD^\dagger)^{-1}, \\ D &= \begin{pmatrix} \frac{-\chi + i\Delta - i\sqrt{\tau}}{\alpha_2'\omega_1} & \frac{-\chi + i\Delta + i\sqrt{\tau}}{\alpha_2'\omega_1} \\ 1 & 1 \end{pmatrix}, \\ \tau &= \Delta^2 - \chi^2 + 2i\Delta\chi - \alpha_1'\alpha_2'\omega_1\omega_2, \end{aligned} \tag{12}$$

with D being the diagonalizing matrix for H_0. In phase 2, H_0 satisfies $\tilde{\eta} H_0 \tilde{\eta}^{-1} = H_0^\dagger$, one of the forms of the metric $\tilde{\eta}$ is

$$\tilde{\eta} = (D\sigma_x D^\dagger)^{-1}. \tag{13}$$

For simplicity, we use Pauli matrix to describe the (anti-)pseudo-Hermiticity and the corresponding (anti-)TRS† symmetry [78] for $\chi = 0$ and $\Delta = 0$, respectively, as shown in Table I. The (anti-)TRS† symmetry also gives rise to (anti-)$\mathcal{PT}$ symmetry [46,81] (where $P = \sigma_{x,y}$ and $T = \mathcal{K}_0$, $\mathcal{K}_0$ is the complex-conjugation operator) with $|\alpha_1'\omega_2| = |\alpha_2'\omega_1|$ (it is $\alpha_1'\omega_2 = \alpha_2'\omega_1$ in our system resulted in anti-$\mathcal{PT}$ symmetry) being a special case.

IV. EQUALLY (UNEQUALLY) ENHANCED SPIN-WAVE EXCITATION ON THE EXCEPTIONAL LINE WITH ANTI-$\mathcal{PT}$ SYMMETRY UNBROKEN (BROKEN)

As indicated in the last section, the EL acts as a dividing line between the pseudo-Hermitian phase 1 and phase 2. Discrete spectra of an η-pseudo-Hermitian Hamiltonian would merge into one at EL for both real and imaginary parts. Unlike the general degenerate points, the eigenstates of the two levels become one at the EP (EL). Thus, physical properties are usually more sensitive to the parameter changes at EP (EL)

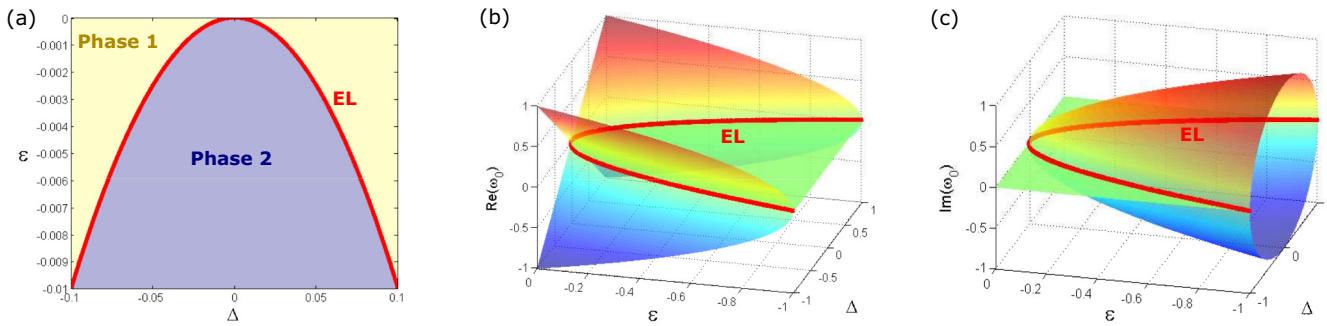

FIG. 3. (a) Pseudo-Hermitian phase diagram for $\chi = 0$: phase 1 (blue), phase 2 (yellow), EL (red). The (b) real and (c) imaginary parts of the spectrum for $\chi = 0$

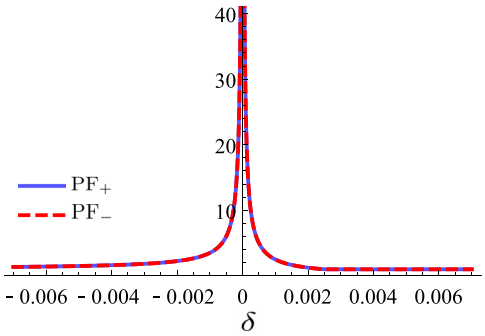

FIG. 4. The Petermann factor PF_+, PF_- near EL, evaluated at $|\Delta| = 0.05$, $|\alpha_1'\omega_2| \approx |\alpha_2'\omega_1|$. $\delta = \Delta^2 + \varepsilon$ denotes the difference between the calculated state and EL in $\chi = 0$ plane.

[6,82–84]. In our system, the EL reads

$$\Delta^2 + \varepsilon = 0, \quad \chi = 0, \tag{14}$$

where the detuning equals to the enhanced damping in order of magnitude, resulting in a full compensation mechanism. Now, we focus on the physical properties of the pseudo-Hermitian states near EL.

For $\chi = 0$, H_0 becomes

$$H_0|_{\chi=0} = \begin{pmatrix} \Delta & -i\alpha_1'\omega_2 \\ -i\alpha_2'\omega_1 & -\Delta \end{pmatrix}, \tag{15}$$

with the bi-orthogonal basis being

$$|\phi_\pm^R\rangle = \begin{pmatrix} \frac{i\Delta \pm i\sqrt{\Delta^2+\varepsilon}}{\alpha_2'\omega_1} \\ 1 \end{pmatrix},$$
$$|\phi_\pm^L\rangle = \begin{pmatrix} \frac{-i\Delta \mp i(\sqrt{\Delta^2+\varepsilon})^*}{\alpha_1'\omega_2} \\ 1 \end{pmatrix}, \tag{16}$$

where

$$\langle\phi_+^L|\phi_-^R\rangle = \langle\phi_-^L|\phi_+^R\rangle = 0,$$
$$\frac{|\phi_+^L\rangle\langle\phi_+^R|}{\langle\phi_+^L|\phi_+^R\rangle} + \frac{|\phi_-^L\rangle\langle\phi_-^R|}{\langle\phi_-^L|\phi_-^R\rangle} = \mathbb{I}. \tag{17}$$

The two eigenstates becomes self-orthogonal on EL: $\langle\phi_\pm^L|\phi_\pm^R\rangle\,|_{\rm EL} = 0$. To characterize the properties near EL, we calculate the Petermann factor (a measure of non-orthogonality, which so far has been shown to diverge at the EPs of optical systems [84,85], and we find that its mathematical expression is also applicable to non-Hermitian spin-wave systems), i.e., the excess spontaneous emission factor [84,86,87] of the system

$$\mathrm{PF}_\pm = \frac{\langle\phi_\pm^L|\phi_\pm^L\rangle\langle\phi_\pm^R|\phi_\pm^R\rangle}{|\langle\phi_\pm^L|\phi_\pm^R\rangle|^2}, \tag{18}$$

as a function of $\delta = \Delta^2 + \varepsilon$, where δ describes the "distance" of the state from EL in the $\chi = 0$ plane. The result is shown in Fig. 4, where $\mathrm{PF}_\pm$ diverges at EL (the $\delta = 0$ point). The divergence of Petermann factor is usually associated with the enhanced excitations of particles [84,85,88]. Upon discovering the EL, we regress the analysis of pseudo-Hermiticity and symmetries of H_0 to the entire dynamics of the system. Thus, we calculate $m_{i\perp}$ as a function of precession frequency ω by introducing a small circularly polarized resonance field $h_i e^{-i\omega t}$ into F_i. The effective magnetic fields becomes $H_{\mathrm{eff},i} + h_i e^{-i\omega t}$, and the dynamic equations becomes

$$\Omega\begin{pmatrix} m_{1\perp} \\ m_{2\perp} \end{pmatrix} = \begin{pmatrix} -\gamma_1 h_1 \\ -\gamma_2 h_2 \end{pmatrix}. \tag{19}$$

We plot the corresponding resonance in Fig. 5, for states at EP, phase 1 and phase 2, respectively, by slightly different $\omega_1 = 1.08,\ 1.1,\ 1.12$, when other parameters are identical.

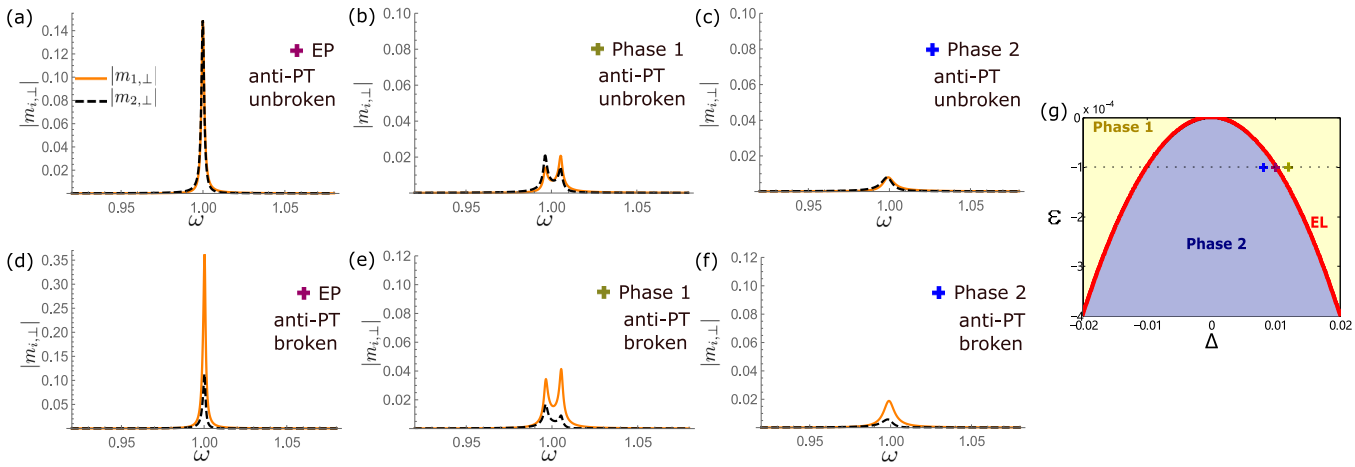

FIG. 5. The perpendicular component of magnetization direction $|m_{i,\perp}|$ as a function of frequency of the circularly polarized resonance field ω when resonance occurs. Panels (a)–(c) describe the situations when $\alpha_1'\omega_2/\alpha_2'\omega_1 = 1$ (anti-$\mathcal{PT}$ symmetry unbroken): (a) Resonance at an EP ($\omega_1 = 1.01$). (b) Resonance at phase 1 ($\omega_1 = 1.012$). (c) Resonance at phase 2 ($\omega_1 = 1.008$), with the same $\omega_2 = 0.99$, $\alpha_1' = 0.0101$, $\alpha_2' = 0.0099$, $\alpha_i = -0.9\alpha_i'$, $\gamma_i h_i = 10^{-5}$ for panels (a)–(c). Panels (d)–(f) describe the cases when $\alpha_1'\omega_2/\alpha_2'\omega_1 = 10$ (anti-$\mathcal{PT}$ symmetry broken), with the same ω_i, $\gamma_i h_i$ as in panels (a)–(c) but $\alpha_1' = 0.0319$, $\alpha_2' = 0.0031$, $\alpha_1 = -0.0309$, $\alpha_2 = -0.0021$. The above parameter settings satisfy $\chi \simeq 0$ (pseudo-Hermitian), and a global damping of $i\mathcal{A} = 0.001$ is induced in all six modes. Here, (a), (d) $\delta = 0$; (b), (e) $\delta = 4.4 \times 10^{-5}$; (c), (f) $\delta = -3.6 \times 10^{-5}$ determines the different phases of these states, which we mark by purple, dark-green, and blue signs in the pseudo-Hermitian ($\chi = 0$) phase diagram (g), respectively.

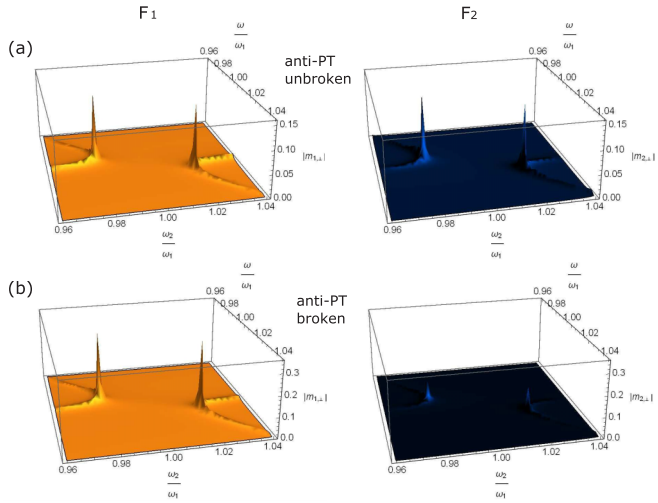

FIG. 6. The perpendicular components of magnetization direction $|m_{1,\perp}|$ (left) and $|m_{2,\perp}|$ (right) as functions of ω_2/ω_1 and ω/ω_1 when $\varepsilon = -10^{-4}$, $\gamma_i h_i/\omega_1 = 10^{-5}$. (a) $\alpha_1'\omega_2/\alpha_2'\omega_1 = 1$ (anti-$\mathcal{PT}$ symmetry unbroken), $\alpha_1' = 0.01/\omega_2$, $\alpha_2' = 0.01/\omega_1$, $\alpha_i = -0.9\alpha_i'$. (b) $\alpha_1'\omega_2/\alpha_2'\omega_1 = 10$ (anti-$\mathcal{PT}$ symmetry broken), $\alpha_1' = (0.01/\omega_2)\sqrt{10}$, $\alpha_2' = (0.01/\omega_1)\sqrt{10}$, $\alpha_1 = -\alpha_1' + 0.001/\omega_2$, $\alpha_2 = -\alpha_2' + 0.001/\omega_1$.

A small global damping $i\mathcal{A}$ is induced in all cases in order to conform to actual possible interferences. Here we have introduce a negative Gilbert damping ($\alpha_i < 0$) to ensure a small enough $i\mathcal{A}$ when $\chi = 0$, which can be realized via STT. From Figs. 5(a)–5(c), the response is grossly sensitive to slightly adjustment of ω_1, and the spin-wave excitation is enhanced at EPs. Possible applications of this result are, for example, high-sensitivity sensors for magnetic-field fluctuation, coherent perfect absorption of spin waves, detection of weak electromagnetic signals, magnon generators with stable frequency and extremely narrow linewidths in quantum circuits, magnetic-field-controlled binary signal switching, etc.

A more intriguing result can be obtained by comparing Figs. 5(a)–5(c) with Figs. 5(d)–5(f): The system holds anti-$\mathcal{PT}$ symmetry for $\alpha_1'\omega_2 = \alpha_2'\omega_1$, $|m_{1,\perp}|/|m_{2,\perp}| = 1$ as shown in Figs. 5(a)–5(c), while the anti-$\mathcal{PT}$ symmetry is broken for $\alpha_1'\omega_2 \neq \alpha_2'\omega_1$, $|m_{1,\perp}|/|m_{2,\perp}| \neq 1$ as shown in Figs. 5(d)–5(f). The perpendicular (to $H_{\text{eff},i}$) component of magnetization direction $|m_{i,\perp}|$ which characterize the intensity of the spin-wave excitation follows the rule that $|m_{1,\perp}|/|m_{2,\perp}| = \sqrt{\alpha_1'\omega_2/\alpha_2'\omega_1}$ for small-angle excitations around EL. By adjusting the ratio of α_1' and α_1' properly, the spin-wave excitation can be imbalanced in the two subsystems, or even occurs only in one of the ferromagnets when $\alpha_i'/\alpha_j' \to \infty$.

Figure 6 shows $|m_{i,\perp}|$ as a function of ω_2/ω_1 and ω/ω_1 when the state changes along the doted line in Fig. 5(g), for anti-$\mathcal{PT}$ symmetry unbroken case and the anti-$\mathcal{PT}$ symmetry broken case, respectively. The anti-$\mathcal{PT}$ symmetry unbroken case in Fig. 6(a) and the anti-$\mathcal{PT}$ symmetry broken case in Fig. 6(b) have the same energy level but different excitation status. This result can be applied to the distribution and amplification of monochromatic spin-wave signals.

Although only two EPs are selected for discussions, the EL can provide a wide range of parameter adjustment in experiments. Experimentally, α_i' can be adjusted through changing d_i, the F/N interface area, and the material, to achieve different EPs, where the state only needs to satisfy Eq. (14). A feasible plan is to first determine α_i' of the system, and then adjust $\mathbf{H}_{\text{eff},i}$ and α_i as necessary.

V. CONCLUDING REMARKS

In summary, we have study the pseudo-Hermitian properties of a two-tone driving $F|N|F$ system. The geometric property of spectra and the status of spin-wave excitation can be characterized by pseudo-Hermiticity phase and symmetry of the Hamiltonian. The EL appears between the two phases of the pseudo-Hermitian region with divergently enhanced spin-wave excitation when the negative Gilbert damping is induced. In particular, anti-$\mathcal{PT}$ symmetry unbroken (broken) of the Hamiltonian can result in equally (unequally) spin-wave excitation in two ferromagnets. The results possess an innate physical essence which has the potential to be applied to other physical systems.

ACKNOWLEDGMENT

We wish to acknowledge the financial support from National Natural Science Foundation of China (Basic Science Center Project) (Grant No. 12088101).

[1] C. M. Bender, Making sense of non-Hermitian Hamiltonians, Rep. Prog. Phys. **70**, 947 (2007).
[2] N. Moiseyev, *Non-Hermitian Quantum Mechanics* (Cambridge University Press, 2011).
[3] Y. Ashida, Z. Gong, and M. Ueda, Non-Hermitian physics, Adv. Phys. **69**, 249 (2020).
[4] R. El-Ganainy, K. G. Makris, M. Khajavikhan, Z. H. Musslimani, S. Rotter, and D. N. Christodoulides, Non-Hermitian physics and $\mathcal{PT}$ symmetry, Nat. Phys. **14**, 11 (2018).
[5] L. Feng, R. El-Ganainy, and L. Ge, Non-Hermitian photonics based on parity–time symmetry, Nat. Photonics **11**, 752 (2017).
[6] Q. Liao, C. Leblanc, J. Ren, F. Li, Y. Li, D. Solnyshkov, G. Malpuech, J. Yao, and H. Fu, Experimental Measurement of the Divergent Quantum Metric of an Exceptional Point, Phys. Rev. Lett. **127**, 107402 (2021).
[7] S. Longhi, Parity-time symmetry meets photonics: A new twist in non-Hermitian optics, Europhys. Lett. **120**, 64001 (2017).
[8] M. Pan, H. Zhao, P. Miao, S. Longhi, and L. Feng, Photonic zero mode in a non-Hermitian photonic lattice, Nat. Commun. **9**, 1 (2018).
[9] R. El-Ganainy, M. Khajavikhan, D. N. Christodoulides, and S. K. Ozdemir, The dawn of non-Hermitian optics, Commun. Phys. **2**, 37 (2019).

[10] M. P. Hokmabadi, A. Schumer, D. N. Christodoulides, and M. Khajavikhan, Non-Hermitian ring laser gyroscopes with enhanced Sagnac sensitivity, Nature (London) **576**, 70 (2019).

[11] S. K. Gupta, Y. Zou, X.-Y. Zhu, M.-H. Lu, L.-J. Zhang, X.-P. Liu, and Y.-F. Chen, Parity-time symmetry in non-hermitian complex optical media, Adv. Mater. **32**, 1903639 (2020).

[12] W. Cao, X. Lu, X. Meng, J. Sun, H. Shen, and Y. Xiao, Reservoir-Mediated Quantum Correlations in Non-Hermitian Optical System, Phys. Rev. Lett. **124**, 030401 (2020).

[13] K. Wang, L. Xiao, J. C. Budich, W. Yi, and P. Xue, Simulating Exceptional Non-Hermitian Metals with Single-Photon Interferometry, Phys. Rev. Lett. **127**, 026404 (2021).

[14] A. Steinfurth, I. Krešić, S. Weidemann, M. Kremer, K. G. Makris, M. Heinrich, S. Rotter, and A. Szameit, Observation of photonic constant-intensity waves and induced transparency in tailored non-Hermitian lattices, Sci. Adv. **8**, eabl7412 (2022).

[15] H. Yuan, Y. Cao, A. Kamra, R. A. Duine, and P. Yan, Quantum magnonics: When magnon spintronics meets quantum information science, Phys. Rep. **965**, 1 (2022).

[16] W. Chen, M. Abbasi, B. Ha, S. Erdamar, Y. N. Joglekar, and K. W. Murch, Decoherence-Induced Exceptional Points in a Dissipative Superconducting Qubit, Phys. Rev. Lett. **128**, 110402 (2022).

[17] Y. Wang, W. Xiong, Z. Xu, G.-Q. Zhang, and J.-Q. You, Dissipation-induced nonreciprocal magnon blockade in a magnon-based hybrid system, Sci. China Math. **65**, 1 (2022).

[18] M. Naghiloo, M. Abbasi, Y. N. Joglekar, and K. Murch, Quantum state tomography across the exceptional point in a single dissipative qubit, Nat. Phys. **15**, 1232 (2019).

[19] J. Cen and A. Saxena, Anti-$\mathcal{PT}$-symmetric qubit: Decoherence and entanglement entropy, Phys. Rev. A **105**, 022404 (2022).

[20] Y. Tabuchi, S. Ishino, A. Noguchi, T. Ishikawa, R. Yamazaki, K. Usami, and Y. Nakamura, Coherent coupling between a ferromagnetic magnon and a superconducting qubit, Science **349**, 405 (2015).

[21] W. Chen, M. Abbasi, Y. N. Joglekar, and K. W. Murch, Quantum Jumps in the Non-Hermitian Dynamics of a Superconducting Qubit, Phys. Rev. Lett. **127**, 140504 (2021).

[22] Y. Chu, Y. Liu, H. Liu, and J. Cai, Quantum Sensing with a Single-Qubit Pseudo-Hermitian System, Phys. Rev. Lett. **124**, 020501 (2020).

[23] R. Grimaudo, A. Messina, A. Sergi, N. V. Vitanov, and S. N. Filippov, Two-qubit entanglement generation through non-Hermitian Hamiltonians induced by repeated measurements on an ancilla, Entropy **22**, 1184 (2020).

[24] R. Lebrun, S. Tsunegi, P. Bortolotti, H. Kubota, A. Jenkins, M. Romera, K. Yakushiji, A. Fukushima, J. Grollier, S. Yuasa *et al.*, Mutual synchronization of spin torque nano-oscillators through a long-range and tunable electrical coupling scheme, Nat. Commun. **8**, 15825 (2017).

[25] V. L. Grigoryan and K. Xia, Thermally induced monochromatic microwave generation in magnon polaritons, Phys. Rev. B **99**, 224408 (2019).

[26] D. Zhang, X.-Q. Luo, Y.-P. Wang, T.-F. Li, and J. You, Observation of the exceptional point in cavity magnon-polaritons, Nat. Commun. **8**, 1 (2017).

[27] H. Y. Yuan, P. Yan, S. Zheng, Q. Y. He, K. Xia, and M.-H. Yung, Steady Bell State Generation via Magnon-Photon Coupling, Phys. Rev. Lett. **124**, 053602 (2020).

[28] V. L. Grigoryan and K. Xia, Cavity-mediated dissipative spin-spin coupling, Phys. Rev. B **100**, 014415 (2019).

[29] V. L. Grigoryan, K. Shen, and K. Xia, Synchronized spin-photon coupling in a microwave cavity, Phys. Rev. B **98**, 024406 (2018).

[30] M. Harder, Y. Yang, B. M. Yao, C. H. Yu, J. W. Rao, Y. S. Gui, R. L. Stamps, and C.-M. Hu, Level Attraction Due to Dissipative Magnon-Photon Coupling, Phys. Rev. Lett. **121**, 137203 (2018).

[31] W. Yu, J. Wang, H. Y. Yuan, and J. Xiao, Prediction of Attractive Level Crossing via a Dissipative Mode, Phys. Rev. Lett. **123**, 227201 (2019).

[32] J. Zhao, Y. Liu, L. Wu, C.-K. Duan, Y.-x. Liu, and J. Du, Observation of anti-$\mathcal{PT}$-symmetry phase transition in the magnon-cavity-magnon coupled system, Phys. Rev. Appl. **13**, 014053 (2020).

[33] V. L. Grigoryan and K. Xia, Pseudo-Hermitian magnon-polariton system with a three-dimensional exceptional surface, Phys. Rev. B **106**, 014404 (2022).

[34] S. Tsunegi, T. Taniguchi, K. Nakajima, S. Miwa, K. Yakushiji, A. Fukushima, S. Yuasa, and H. Kubota, Physical reservoir computing based on spin torque oscillator with forced synchronization, Appl. Phys. Lett. **114**, 164101 (2019).

[35] R. Santra and L. S. Cederbaum, Non-Hermitian electronic theory and applications to clusters, Phys. Rep. **368**, 1 (2002).

[36] J.-H. Zhang and F.-Q. Dou, High-fidelity formation of deeply bound ultracold molecules via non-Hermitian shortcut to adiabaticity, New J. Phys. **23**, 063001 (2021).

[37] Z.-Q. Fu, Y. Pan, J.-J. Zhou, K.-K. Bai, D.-L. Ma, Y. Zhang, J.-B. Qiao, H. Jiang, H. Liu, and L. He, Relativistic artificial molecules realized by two coupled graphene quantum dots, Nano Lett. **20**, 6738 (2020).

[38] M. Ernzerhof, A. Giguère, and D. Mayou, Non-Hermitian quantum mechanics and exceptional points in molecular electronics, J. Chem. Phys. **152**, 244119 (2020).

[39] T. Kato, Wave operators and similarity for some non-selfadjoint operators, Math. Ann. **162**, 258 (1966).

[40] W. Heiss, The physics of exceptional points, J. Phys. A: Math. Theor. **45**, 444016 (2012).

[41] N. Hatano and D. R. Nelson, Localization Transitions in Non-Hermitian Quantum Mechanics, Phys. Rev. Lett. **77**, 570 (1996).

[42] C. M. Bender and S. Boettcher, Real Spectra in Non-Hermitian Hamiltonians Having $\mathcal{PT}$ Symmetry, Phys. Rev. Lett. **80**, 5243 (1998).

[43] C. M. Bender, S. Boettcher, and P. N. Meisinger, $\mathcal{PT}$-symmetric quantum mechanics, J. Math. Phys. **40**, 2201 (1999).

[44] A. Mostafazadeh, Pseudo-Hermitian representation of quantum mechanics, Int. J. Geom. Methods Mod. Phys. **07**, 1191 (2010).

[45] A. Mostafazadeh and A. Batal, Physical aspects of pseudo-Hermitian and $\mathcal{PT}$-symmetric quantum mechanics, J. Phys. A: Math. Gen. **37**, 11645 (2004).

[46] A. Mostafazadeh, Pseudo-Hermiticity versus $\mathcal{PT}$ symmetry: The necessary condition for the reality of the spectrum of a non-Hermitian Hamiltonian, J. Math. Phys. **43**, 205 (2002).

[47] Y. Tserkovnyak, Exceptional points in dissipatively coupled spin dynamics, Phys. Rev. Res. **2**, 013031 (2020).

[48] R. Okugawa and T. Yokoyama, Topological exceptional surfaces in non-Hermitian systems with parity-time and parity-particle-hole symmetries, Phys. Rev. B **99**, 041202(R) (2019).

[49] Y. Tserkovnyak, A. Brataas, and G. E. W. Bauer, Spin pumping and magnetization dynamics in metallic multilayers, Phys. Rev. B **66**, 224403 (2002).
[50] B. Heinrich, Y. Tserkovnyak, G. Woltersdorf, A. Brataas, R. Urban, and G. E. W. Bauer, Dynamic Exchange Coupling in Magnetic Bilayers, Phys. Rev. Lett. **90**, 187601 (2003).
[51] T. Taniguchi and H. Imamura, Enhancement of the Gilbert damping constant due to spin pumping in noncollinear ferromagnet/nonmagnet/ferromagnet trilayer systems, Phys. Rev. B **76**, 092402 (2007).
[52] P. Bruno, Theory of interlayer magnetic coupling, Phys. Rev. B **52**, 411 (1995).
[53] S. D. Bader, Colloquium: Opportunities in nanomagnetism, Rev. Mod. Phys. **78**, 1 (2006).
[54] U. Rücker, S. Demokritov, E. Tsymbal, P. Grünberg, and W. Zinn, Biquadratic coupling in Fe/Au/Fe trilayers: Experimental evidence for the magnetic-dipole mechanism, J. Appl. Phys. **78**, 387 (1995).
[55] J. M. Lee, T. Kottos, and B. Shapiro, Macroscopic magnetic structures with balanced gain and loss, Phys. Rev. B **91**, 094416 (2015).
[56] H. Liu, D. Sun, C. Zhang, M. Groesbeck, R. Mclaughlin, and Z. V. Vardeny, Observation of exceptional points in magnonic parity-time symmetry devices, Sci. Adv. **5**, eaax9144 (2019).
[57] T. Yu, H. Yang, L. Song, P. Yan, and Y. Cao, Higher-order exceptional points in ferromagnetic trilayers, Phys. Rev. B **101**, 144414 (2020).
[58] Y. Tserkovnyak, A. Brataas, and G. E. W. Bauer, Enhanced Gilbert Damping in Thin Ferromagnetic Films, Phys. Rev. Lett. **88**, 117601 (2002).
[59] Y. Tserkovnyak, A. Brataas, G. E. W. Bauer, and B. I. Halperin, Nonlocal magnetization dynamics in ferromagnetic heterostructures, Rev. Mod. Phys. **77**, 1375 (2005).
[60] S. Kaka, M. R. Pufall, W. H. Rippard, T. J. Silva, S. E. Russek, and J. A. Katine, Mutual phase-locking of microwave spin torque nano-oscillators, Nature (London) **437**, 389 (2005).
[61] F. Mancoff, N. Rizzo, B. Engel, and S. Tehrani, Phase-locking in double-point-contact spin-transfer devices, Nature (London) **437**, 393 (2005).
[62] S. Komineas, Non-Hermitian dynamics of a two-spin system with PT symmetry, Phys. Rev. B **107**, 094435 (2023).
[63] G. L. Giorgi, F. Plastina, G. Francica, and R. Zambrini, Spontaneous synchronization and quantum correlation dynamics of open spin systems, Phys. Rev. A **88**, 042115 (2013).
[64] J. Grollier, V. Cros, and A. Fert, Synchronization of spin-transfer oscillators driven by stimulated microwave currents, Phys. Rev. B **73**, 060409(R) (2006).
[65] S. Tsunegi, T. Taniguchi, R. Lebrun, K. Yakushiji, V. Cros, J. Grollier, A. Fukushima, S. Yuasa, and H. Kubota, Scaling up electrically synchronized spin torque oscillator networks, Sci. Rep. **8**, 13475 (2018).
[66] P. P. Orth, D. Roosen, W. Hofstetter, and K. Le Hur, Dynamics, synchronization, and quantum phase transitions of two dissipative spins, Phys. Rev. B **82**, 144423 (2010).
[67] S. Sani, J. Persson, S. M. Mohseni, Y. Pogoryelov, P. Muduli, A. Eklund, G. Malm, M. Käll, A. Dmitriev, and J. Åkerman, Mutually synchronized bottom-up multi-nanocontact spin–torque oscillators, Nat. Commun. **4**, 2731 (2013).
[68] B. G. Simon, S. Kurdi, H. La, I. Bertelli, J. J. Carmiggelt, M. Ruf, N. De Jong, H. Van Den Berg, A. J. Katan, and T. van der Sar, Directional excitation of a high-density magnon gas using coherently driven spin waves, Nano Lett. **21**, 8213 (2021).
[69] K. Lenz, T. Toliński, J. Lindner, E. Kosubek, and K. Baberschke, Evidence of spin-pumping effect in the ferromagnetic resonance of coupled trilayers, Phys. Rev. B **69**, 144422 (2004).
[70] S. Rezende, R. Rodríguez-Suárez, M. Soares, L. Vilela-Leão, D. Ley Domínguez, and A. Azevedo, Enhanced spin pumping damping in yttrium iron garnet/Pt bilayers, Appl. Phys. Lett. **102**, 012402 (2013).
[71] T. Moriyama, S. Takei, M. Nagata, Y. Yoshimura, N. Matsuzaki, T. Terashima, Y. Tserkovnyak, and T. Ono, Anti-damping spin transfer torque through epitaxial nickel oxide, Appl. Phys. Lett. **106**, 162406 (2015).
[72] A. Hamadeh, O. d'Allivy Kelly, C. Hahn, H. Meley, R. Bernard, A. H. Molpeceres, V. V. Naletov, M. Viret, A. Anane, V. Cros, S. O. Demokritov, J. L. Prieto, M. Munoz, G. de Loubens, and O. Klein, Full Control of the Spin-Wave Damping in a Magnetic Insulator Using Spin-Orbit Torque, Phys. Rev. Lett. **113**, 197203 (2014).
[73] A. I. Nikitchenko and N. A. Pertsev, Spin-orbit torque control of spin waves in a ferromagnetic waveguide, Phys. Rev. B **104**, 134422 (2021).
[74] J. Xiao, G. E. W. Bauer, K. C. Uchida, E. Saitoh, and S. Maekawa, Theory of magnon-driven spin Seebeck effect, Phys. Rev. B **81**, 214418 (2010).
[75] K. Uchida, S. Takahashi, K. Harii, J. Ieda, W. Koshibae, K. Ando, S. Maekawa, and E. Saitoh, Observation of the spin Seebeck effect, Nature (London) **455**, 778 (2008).
[76] D. Gall, Electron mean free path in elemental metals, J. Appl. Phys. **119**, 085101 (2016).
[77] See Supplemental Material http://link.aps.org/supplemental/10.1103/PhysRevB.108.064428 for the estimation when the static coupling is sizable; the spectral matching of the coupled LLG equations and the Hamiltonian; and a derivation of the coalescent length of the spectrum when $\chi = 0$. The Supplemental Material also contains Refs. [50,52,69].
[78] K. Kawabata, K. Shiozaki, M. Ueda, and M. Sato, Symmetry and Topology in Non-Hermitian Physics, Phys. Rev. X **9**, 041015 (2019).
[79] R. Zhang, H. Qin, and J. Xiao, $\mathcal{PT}$-symmetry entails pseudo-Hermiticity regardless of diagonalizability, J. Math. Phys. **61**, 012101 (2020).
[80] F. Kleefeld, Identification of the metric for diagonalizable (anti-) pseudo-hermitian hamilton operators represented by two-dimensional matrices, arXiv:2102.08182.
[81] Z. Ahmed, C-, PT- and CPT-invariance of pseudo-Hermitian Hamiltonians, J. Phys. A: Math. Gen. **36**, 9711 (2003).
[82] V. L. Grigoryan and K. Xia, Torque-induced dispersive readout in a weakly coupled hybrid system, Phys. Rev. B **102**, 064426 (2020).
[83] Y.-H. Lai, Y.-K. Lu, M.-G. Suh, Z. Yuan, and K. Vahala, Observation of the exceptional-point-enhanced Sagnac effect, Nature (London) **576**, 65 (2019).
[84] Z. Lin, A. Pick, M. Lončar, and A. W. Rodriguez, Enhanced Spontaneous Emission at Third-Order Dirac Exceptional Points in Inverse-Designed Photonic Crystals, Phys. Rev. Lett. **117**, 107402 (2016).
[85] S.-Y. Lee, J.-W. Ryu, J.-B. Shim, S.-B. Lee, S. W. Kim, and K. An, Divergent Petermann factor of interacting resonances

in a stadium-shaped microcavity, Phys. Rev. A **78**, 015805 (2008).

[86] K. Petermann, Calculated spontaneous emission factor for double-heterostructure injection lasers with gain-induced waveguiding, IEEE J. Quantum Electron. **15**, 566 (1979).

[87] L. Ferrier, P. Bouteyre, A. Pick, S. Cueff, N. H. M. Dang, C. Diederichs, A. Belarouci, T. Benyattou, J. X. Zhao, R. Su, J. Xing, Q. Xiong, and H. S. Nguyen, Unveiling the Enhancement of Spontaneous Emission at Exceptional Points, Phys. Rev. Lett. **129**, 083602 (2022).

[88] H. Wang, Y.-H. Lai, Z. Yuan, M.-G. Suh, and K. Vahala, Petermann-factor sensitivity limit near an exceptional point in a Brillouin ring laser gyroscope, Nat. Commun. **11**, 1610 (2020).